Published in final edited form as:
Neurobiol Dis. 2013 October ; 58: 281–288. doi:10.1016/j.nbd.2013.06.010.

Complex I inhibition in the visual pathway induces disorganization of the node of Ranvier

Mathieu Marella, **Gaurav Patki**, **Akemi Matsuno-Yagi**, and **Takao Yagi**
Department of Molecular and Experimental Medicine, MEM-256, The Scripps Research Institute, 10550 N. Torrey Pines Rd., La Jolla, California 92037, U.S.A

Abstract

Mitochondrial defects can have significant consequences on many aspects of neuronal physiology. In particular, deficiencies in the first enzyme complex of the mitochondrial respiratory chain (complex I) are considered to be involved in a number of human neurodegenerative diseases. The current work highlights a tight correlation between the inhibition of complex I and the state of axonal myelination of the optic nerve. Exposing the visual pathway of rats to rotenone, a complex I inhibitor, resulted in disorganization of the node of Ranvier. The structure and function of the node depends on specific cell adhesion molecules, among others, CASPR (contactin associated protein) and contactin. CASPR and contactin are both on the axonal surface and need to be associated to be able to anchor their myelin counter part. Here we show that inhibition of mitochondrial complex I by rotenone in rats induces reactive oxygen species, disrupts the interaction of CASPR and contactin couple, and thus damages the organization and function of the node of Ranvier. Demyelination of the optic nerve occurs as a consequence which is accompanied by a loss of vision. The physiological impairment could be reversed by introducing an alternative NADH dehydrogenase to the mitochondria of the visual system. The restoration of the nodal structure was specifically correlated with visual recovery in the treated animal.

Keywords

mitochondrial complex I; neurodegenerative disease; visual pathway; myelination; node of Ranvier; optic neuropathy

Introduction

Mitochondria are intracellular organelles that produce most of the molecular energy (ATP) and are also involved in cellular physiology such as Ca^{2+} homeostasis, reactive oxygen species (ROS) signaling and apoptosis (Smith et al., 2012; Murphy, 2009). Because of their central role, the dysfunction of mitochondria leads to a diversity of disorders spanning from neurodegenerative diseases to diabetes, myopathies and cardiomyopathies (Correia et al., 2012; Joseph et al., 2012; Nunnari and Suomalainen, 2012). The mitochondrial oxidative phosphorylation system consists of five enzyme complexes. The first enzyme complex (NADH:quinone oxidoreductase or complex I) oxidizes NADH and feeds electrons to the

Address correspondence to: Takao Yagi, The Scripps Research Institute, Department of Molecular and Experimental Medicine, 10550 N. Torrey Pines Rd., MEM256, La Jolla, CA 92037 U.SA., Fax: (858) 784-2054, yagi@scripps.edu.

rest of the respiratory chain. At the sites of complexes I, III and IV protons are pumped through the membrane and a fifth complex, the ATP synthase, utilizes this proton motive force to produce ATP. Mitochondria have their own DNA (mtDNA). It codes for 13 subunits of the enzyme complexes, of which 7 are in complex I. Many of the so-called mitochondrial diseases are directly linked to complex I deficiencies. Malfunction of complex I could lead to generation of massive amounts of ROS at the site of this enzyme complex (Drose and Brandt, 2012). Human diseases that are considered to be related to dysfunctions of complex I, either directly or indirectly, include neurodegenerative disorders such as Parkinson's disease, Leigh syndrome, Leber's hereditary optic neuropathy (LHON), mitochondrial encephalopathy, lactic acidosis and stroke-like episodes (MELAS) (Schapira, 1998; Sproule and Kaufmann, 2008; Filosto et al., 2007).

In order to assess the pathophysiological events linked to complex I dysfunction in animals we exposed the visual pathway of rats to rotenone. Rotenone is a very potent and specific complex I inhibitor that has been already used to decipher disease pathophysiology in animals (Sherer et al., 2007; Zhang et al., 2002). This complex I inhibitor is highly hydrophobic and can therefore cross biological membranes. In the visual pathway, ganglion cells of the retina have axons that span from the eyecup up to their main projection site in the superior colliculus (SC) of the brain. The transmission of neural information over such a long distance relies on elaborated structures. In the optic nerve, axons are tightly covered by layers of myelin derived from expansion of oligodendrocyte membranes. Myelinated axons can conduct action potentials at great speed and with high efficiency. This is enabled by the presence of the node of Ranvier, a small set of gaps within the myelin sheath that leaves portions of axon completely uncovered (Hildebrand et al., 1993). The node of Ranvier renders possible a unique mode of excitation called saltatory conduction (Salzer, 2003). The gaps are structurally well defined with juxtaparanode and paranode surrounding the uncovered section of the axon. The paranode is the location where the myelin sheath ends. It contains specific anchorage proteins such as CASPR (contactin associated protein) and contactin that bond the paranodal myelin loops to the axons (Kazarinova-Noyes and Shrager, 2002; Labasque and Faivre-Sarrailh, 2009). In the part of the axon left uncovered, sodium channels are gathered and are mainly responsible for the membrane depolarization. In the optic nerve, a large amount of mitochondria are clustered within the paranodal region of the axon. Therefore this location seems to bear a high vulnerability to metabolic dysfunctions.

In the current work, we observed, upon rotenone exposure, disorganization of the node of Ranvier as well as demyelination of the axons in the visual pathway. Protein and DNA showed a heavy sign of oxidative damage. Complex I dysfunction seems enough to trigger loss of myelination and to induce the invasion of microglial cell in the tissue. This study provides a clue that links complex I dysfunction to demyelinating disorders.

Materials and Methods

Production of rotenone microspheres, treatment of rats with rotenone beads, and behavioral study

Biodegradable microspheres were used to achieve a steady and continuous release of rotenone as detailed previously (Marella et al., 2008). Preparation of rotenone-loaded microspheres was slightly modified as follows: 250 mg of rotenone was dissolved with 300 mg of poly(DL-lactide-co-glycolide) (PLGA) (Sigma, lactide:glycolide 50:50) in 15 ml of dichloromethane. The organic phase was poured into ice-cold 8% (w/v) polyvinyl alcohol (hot water soluble; Sigma). The microspheres were collected by centrifugation and washed with sterile distilled water. The average size of the beads was estimated to be ~6 μm. Long Evans male rats weighing 200 to 250 g (7 week old) (Charles River, Reno) were used for

this study. The animals were housed 2 per cage in a 12 hours light/dark cycle and were fed with food and water *ad libitum*. All procedures were approved by the Institutional Animal Care and Use Committee (IACUC) at The Scripps Research Institute (approval ID 08-0065). The stereotaxic surgery was performed as previously described (Marella et al., 2010). Each animal received a bilateral injection with 3 μl of rotenone-loaded microsphere suspension and/or 3 μl of rAAV2-NDI1 (Boston center) into the optical layer of the SC (coordinates from the Bregma: antero-posterior −0.63 cm; media-lateral ±0.15 cm; dorso-ventral −0.36 cm). As the control empty rAAV2 or PBS was injected. The visual capacity of rats was assessed with the optokinetic test as previously published (Marella et al., 2010). Briefly, the rats were placed in an acrylic cage surrounded by four monitor screens on which patterns of white and black strips were displayed. The rats were monitored for head tracking reflexes (when the motion of the head follows the strip movement) for two minutes. Data were compiled into a graph showing the change in the duration of head tracking over the period of time of the experiment.

Electron microscopy

Rats were euthanized by injection of a high dose of Pentothal, followed by transcardiac perfusion of sterile PBS followed by a fixative solution (1% paraformaldehyde, 3% glutaraldehyde 1 mM calcium chloride, 0.1 M cacodylate). The optic nerves were dissected, washed with PBS, and postfixed in 1% OsO_4, 0.1 M cacodylate, and 3.5% sucrose. Tissues were dehydrated and embedded in Embed 812/Araldite (Electron Microscopy Sciences). Sagittal thin sections (60 nm) of the optic nerves were cut with a diamond knife (Diatome), mounted on copper slot grids coated with parlodion and stained with uranyl acetate and lead citrate for examination on a Philips CM100 electron microscope (FEI, Hillsbrough). Images were documented using a Megaview III ccd camera (Olympus Soft Imaging Solutions).

Immunofluorescence microscopy and staining

The tissue samples were retrieved, fixed in 4% paraformaldehyde and cryoprotected in 20% sucrose in PBS, overnight at 4°C. The eyes and optic nerves were embedded in OCT and sliced using a cryostat at 12 μm (eyes) or 5 μm (optic nerve). Each slice was collected onto Superfrost slides (Fisher) and stored at −20°C. Before staining, a procedure to retrieve antigen was carried out; the microscope slides were microwaved for 10 minutes at 80 - 90°C in 1 mM EDTA, 10 mM Tris-Cl, pH 8. After cooling, the slices were washed in PBS for 10 minutes. The samples were blocked using Tris buffered saline (TBS, pH 7.8) containing 10% bovine serum and 0.1% Triton X-100 for 1 hour and then incubated overnight at 4°C with primary antibodies in TBS, 10% bovine serum, and 0.1% Triton X-100. Primary antibodies were used at the following dilution; 2,4 DNP (1/200), caveolin (1/200), contactin (1/200), Nav1.6 (1/300) and gamma-synuclein (1/200) from Invitrogen, 8-oxo-dG (1/300) from Cosmo Bio Co, Japan, CASPR (1/1000) a generous gift from Dr. Peles (Weizmann Institute, Israel). Histochemical staining for 8-oxo-dG (1/300 dilution, Cosmo Bio Co., Japan) was performed as described before (Marella et al., 2010). Staining with 2,4 DNP antibody was done after the following initial treatment: the tissues were fixed with methacarn (60% methanol, 30% chloroform, 10% glacial acetic acid) for 15 minutes and soaked overnight in 2,4 dinitrophenyl-hydrazine 15 mM, and 1.5% HCl. Slices were washed in a series of baths (2 minutes per bath), ethanol 2%HCl, ethanol 80%, ethanol 100%, ethanol 50%/ethyl Acetate 50%, ethanol 80%, ethanol 50%, and 2 times distilled water. After these washes the slices were blocked and processed as described above. Staining intensity or cell numbers were evaluated with ImageJ software (NIH) (Abramoff et al., 2004). Colocalization was assessed using the Mander's coefficient (Manders et al., 2013): Mander's coefficient ranges between 0 to 1 with 1 representing perfect colocalization.

mRNA analyses by laser capture microdissection

Tissue samples (eyes and optic nerves) were rapidly dissected from the rats and stored on ice in RNAlater (Qiagen) until they were embedded and frozen in OCT to be kept at −80°C. Eight-μm sections were cut in a cryostat and put on untreated glass slides. The samples were immersed in the following baths before micro-dissection; fixation in ethanol 75% for 60 seconds, a wash in water for 30 seconds, a quick dip in hematoxylin, a wash in water for 30 seconds, and a dehydration in 70%, 95%, and 100% ethanol for 35 seconds each. The samples were kept in xylene until the laser micro-dissection. The laser dissection was performed on an Arcturus PixCell II laser capture microdissection attached to an Olympus IX 50 inverted microscope. A large laser spot size (30 μm) was used and laser power and pulse duration were set to 50 mW and 10.5 ms, respectively. The ganglion cell layers of 3 retina slices were collected on a CapSure HS. mRNA was extracted using RNaesy microkit (Qiagen) according to the manufacturers instruction. Complementary DNA was obtained using the Moloney murine leukemia virus reverse transcriptase kit supplemented with RNAseOut (Invitrogen). PCR conditions were optimized for linear amplification, allowing direct comparison between samples. Internal control (beta-2 microglobulin) was used to evaluate the reaction efficiency in each trial. The PCR products were separated on 2.5% agarose gels and visualized using SYBRsafe Green (Molecular Probes). DNA bands were quantified using ImageJ software (NIH) (Abramoff et al., 2004). The level of expression of each gene was normalized against one of beta-2 microglobulins.

Detergent-dependent sub-fractionation of the optic nerve

The optic nerves were smashed between two frosted microscope glass slides. The smashed optic nerve was mixed with 150 μl of PBS completed with protease inhibitor EDTA-free (Roche) (PBSi) and centrifuged for 10 minutes in a Beckman Airfuge centrifuge at 22 psi to remove large debris. The supernatant was saved as S0. The pellet was gently resuspended in 100μl of PBSi containing 1% Triton X-100 and incubated on ice for 30 minutes. After centrifugation (Airfuge for 10 minutes at 22 psi) the supernatant was saved as S1. The pellet was resuspended in PBSi containing 0.5% SDS and incubated at room temperature for 15 minutes. After a final round of centrifugation the supernatant was saved as S2 and the pellet was resuspended in PBSi as P. A 20 μl sample of each fraction was analyzed by Western blot. GAPDH was used as loading control and caveolin (protein associated with lipid rafts) and Kv1.2 (protein not associated with lipid rafts) were used to assess the extraction and fractionation efficiency.

Statistics

Data were obtained from at least 3 animals. Experiments were performed on 4 samples per animal repeated 3 times. Errors in the experimental data are presented as ± % standard deviation. Between-group differences were evaluated using one way ANOVA post-hoc test (Graphpad Prism). The significance level was $p \leq 0.05$ or $p \leq 0.01$.

Results

Damages due to rotenone release after PLGA microsphere injection in the superior colliculus (SC) seems to be specific to the retinal ganglion cell layer

Optokinetic test was used to assess the visual ability of the animals exposed to rotenone. The rat's vision was severely impaired at 2 weeks of rotenone exposure and the optokinetic score reached the lowest level in 3 to 4 weeks (Fig. 1A). Activity staining of the tissues showed lowered NADH dehydrogenase (diaphorase) activity in the SC and retina, particularly the ganglion cell layer, after 4weeks of rotenone exposure (Supplementary Fig. 1). The optic nerves project from the retina into the optical layer of the SC, and the visual pathway,

through another projection, continues to the visual cortex (VC). The PLGA injection is carried out at the level of the SC, and because rotenone can cross cell membrane freely we examined the neuronal damage both in the SC and VC by staining sagittal sections of the brain using a neuron specific marker, NeuN (Supplementary Fig. 2). The number of neurons in the SC started to decline 4 weeks postinjection. However, no significant change in the number of neurons was seen in the VC for up to 8 weeks (Fig. 1B). Moreover, the rotenone treatment induced a substantial increase of oxidative insult in the SC over time, whereas, in the VC, the same rotenone treatment did not increase the oxidative insult even after 8 weeks of exposure (Fig. 1C, Supplementary Fig. 3). It seems likely that the retinal ganglion cells comprising the optic nerve are highly susceptible to the rotenone exposure.

One striking feature of the visual loss that takes place during the early phase of rotenone treatment is that the vision can be restored by the action of Ndi1 even 4 weeks after the rotenone injection (Fig. 1A, see also (Marella et al., 2010)). Ndi1 is a single-subunit NADH dehydrogenase found in the mitochondria of yeast *Saccharomyces cerevisiae* that effectively works as an alternative for complex I (Marella et al., 2007; Seo et al., 2006b; Iwata et al., 2012). The time required for the full recovery tended to become longer as the timing of expression of Ndi1 was delayed (from 2 to 3, then to 4 weeks) after rotenone administration (Fig. 1A). As shown previously, expressed Ndi1 works as an alternative dehydrogenase and can bypass defective complex I by re-establishing electron transfer pathway from NADH to the downstream respiratory chain (Marella et al., 2007; Seo et al., 2006a). The present results strongly suggest that the loss of vision is ascribed to the specific action of rotenone on complex I.

Complex I inhibition provoked structural abnormalities of the node of Ranvier

While drastic visual loss occurred during the first 1 to 2 weeks after rotenone injection, no morphological change was observed in the retinal ganglion cell layer or the SC during this period of time. Therefore we closely examined the axon of the optic nerve from the rats. Sections of the optic nerve were stained using antibodies against CASPR and the sodium channel. Fig. 2A displays typical immunostaining images found in the rat visual pathway exposed to rotenone. In a typical (normal) pattern of the node of Ranvier, the CASPR protein is exclusively located at the paranodal region and the sodium channel (Nav1.6) congregates within the nodal gap and is flanked on both sides by CASPR (Fig. 2A, a). This structure is unique and it repeats itself along the axons in the optic nerve. However, in animals exposed to rotenone for 2 weeks, some of the nodes of Ranvier and the paranodal region of the optic nerve have lost their integrity (Fig. 2A, b). The paranode seemed to be invaded by sodium channels and the structure appeared to be fragmented. Such abnormalities were not seen in the axon between the SC and the VC (Supplementary Fig. 4). When the rotenone treatment was prolonged (12 weeks), a majority of the nodes of Ranvier became disorganized. Only a few characteristic patterns were observed and a distorted pattern of staining in the pseudo clustered NaV1.6 and CASPR was evident (Fig. 2A, c). The extent of disorganization of the node of Ranvier was assessed by investigating the morphological properties of CASPR clusters. As the time of rotenone treatment was increased, the total number of CASPR clusters and the average area of those clusters (total surface area of a node of Ranvier) increased significantly (Fig. 2, B and C). The number of disorganized node of Ranvier seems tightly correlated with the progression of visual loss presented in Fig. 1A. It is worth noting here that the chaotic pattern of the node of Ranvier seems to be limited to the CASPR clusters. The potassium channel Kv1.2, which is present in the juxtaparanode, did not undergo the same disorganization. Even with a prolonged rotenone exposure the Kv1.2 clusters seemed to remain intact (Supplementary Fig. 5). In agreement with the results of visual recovery, the disorganization of node of Ranvier was reversed by Ndi1 expression. These data indicate that the observed damage to the node of

Ranvier is derived solely from complex I inhibition and that this structure exhibits substantial plasticity (Fig. 2A, d-f).

Complex I inhibition induced loss of axonal myelination

In order to evaluate the myelination state of the retinal ganglion cell axons, ultrathin sections of optic nerve were examined by electron microscopy. Fig. 3A shows a typical node of Ranvier (marked by a star) surrounded by two distinct paranodal regions (bracketed). The paranode is the region in which the myelin sheath ends to expose the part of the axon responsible for the saltatory conduction of neuronal impulses. In control animals the paranodal region spanned over 4 μm and the uncovered part of the axon had an average length of 1.5 μm. The paranode of the rotenone-treated animals, on the other hand, was much shorter and never exceeded 2 μm. The paranodal region could not be repeated after the node of Ranvier. The mirrored part of the first paranode was missing, leaving the axon uncovered for several micrometers (Fig. 3B). At a higher magnification, the paranodal loop from the control rats showed the classic and specific pattern of septate-like junctions between the myelin sheath and the axon (Fig. 3C). The rotenone-exposed optic nerve displayed a deteriorated paranodal loop of the myelin; the pods were misshaped and swollen (Fig. 3D). Finally, Fig. 3E exhibits inconsistent myelination of a ganglion cell axon that resembles the structure seen in the image of CASPR/Nav1.6 immunofluorescence (Fig. 2A, b). The arrows show myelinated regions intermittently separated by portions of nude axon or covered only by a very thin layer of myelin.

The rotenone treatment resulted in oxidative damages and microglial invasion of the optic nerve

The loss of the myelin and the disorganization of the node of Ranvier were followed by an increase of the microglial population in the optic nerve exposed to rotenone. In Fig. 4 microglial cells were stained using anti-F4/80 antibody as well as anti-CD80 antibody that is more specific for activated macrophages. In control samples, microglia were scarce and displayed a typical form of resting, non-activated cell. The cell body was minimal and extremely ramified. However, their number increased and the shape changed in the optic nerve in animals treated with the complex I inhibitor. The majority of microglia lost their ramification and adopted an amoeboid-shape indicating their activated state (Fig. 4). This microglial invasion of the optic nerve occurred from 3 to 4 weeks after the PLGA-rotenone injection in the SC. This indicates a localized inflammatory response developing along with the visual impairment.

Complex I inhibition by rotenone is known to elicit ROS production (Stefanatos and Sanz, 2011; Marella et al., 2007). To evaluate the oxidative damage caused by the rotenone exposure, the optic nerves were stained using antibodies specific for oxidized protein and nucleic acids. Increase in oxidative damage was observed for both DNA (Fig. 5A) and proteins (Fig. 5B) in the optic nerves with increasing time of rotenone exposure. Here again, mitochondrial expression of Ndi1 was able to reduce the oxidative damage. In addition to the extent of oxidized DNA, there was also a time-dependent change in the location in which the oxidative damage was observed (Supplementary Fig. 6A). After 2 weeks of rotenone exposure mainly the axon (as revealed by gamma synuclein staining) presented a punctiform staining that was indicative of mtDNA oxidation. Then the DNA oxidation signal expanded to the cytoplasm and nuclei of the surrounding cells (mainly astrocytes and oligodendrocytes). The protein oxidation exhibited a similar pattern (Supplementary Fig. 6B). In all cases Ndi1 expression suppressed the effect of rotenone. Fig. 5C illustrates the correlation between the oxidative damage of the mtDNA and the location of the node of Ranvier. While no 8-oxo-dG signal could be revealed in the control sample, the rotenone-

exposed optic nerves displayed a punctiform staining that follows the disorganization of the paranode.

Perturbation of the anchoring mechanism in the paranode region

Several proteins in the axon are involved in myelin anchorage. In the paranodal region two main axonal proteins, CASPR and contactin, play a pivotal role in maintaining the paranodal loop of the oligodendrocytes tightly bond to the neural cells. CASPR and contactin are associated together in the axolemma and are bound to oligodendroglial protein neurofascin 155 located at the base of the paranodal loops. We followed the integrity of the binding between CASPR and contactin in the paranodal region. Fig. 6A summarizes the value of the Mander's coefficients (Manders et al., 2013) evaluating the amount of colocalization between CASPR and contactin. A perfect colocalization will have the value of 1. Under normal conditions, CASPR and contactin were almost totally colocalized with a Mander's coefficient of 0.965±0.026. Rotenone treatment of the rat visual pathway induced a time-dependent loss of the tight association between the two proteins. After 12 weeks of rotenone exposure, more than 25% of the colocalization of CASPR and contactin was lost at the paranode section. Here also, the presence of Ndi1 in the mitochondria was sufficient enough to induce the relocalization of the two proteins. The loss of colocalization between CAPSR and contactin was further investigated using a biochemical method. The procedure takes advantage of the nature of glycophosphatidyl-inositol anchored proteins being sensitive to Triton X-100 extraction (London and Brown, 2000; Schroeder et al., 1998). Contactin is among those anchored proteins known to be integrated in lipid rafts, specific areas of the plasma membrane of cells enriched in sphingolipids. The paranodal region surrounding the node of Ranvier contains a great proportion of lipid rafts (Ogawa and Rasband, 2009). The optic nerves were mashed and were subjected to TritonX-100 extraction. The samples were then separated by centrifugation into a fraction that is mostly devoid of proteins in lipid rafts (S1 in Fig. 6B) and a fraction that contains them (S2 in Fig. 6B). The amounts of CASPR and contactin in S1 were greater in the rotenone-treated animals than that of the control group illustrating the disorganization of the anchorage protein in the paranodal region (Fig. 6B). Caveolin, which is mainly interacting with those lipid rafts, was resistant to the action of TritonX-100. Meanwhile, the majority of potassium channel Kv1.2, a membranous protein not associated with lipid rafts, was susceptible to the Triton X-100 extraction. The histograms show the extent of the Triton X-100 extraction of CASPR and contactin (Fig. 6C).

In order to further identify proteins involved in the structure of the node of Ranvier that could be affected by complex I inhibition, mRNA of the RGC was studied after laser capture micro-dissection (LCM). Thin sections of the retina from the animals exposed to rotenone for 2 weeks were processed through LCM. The level of specific mRNA was tested by reverse transcription-PCR (Fig. 7A). Beta 2 macroglobulin, a housekeeping gene, was used as the standard in all experiments. Clearly, both the Contactin 1 and Contactin 2 genes were inhibited. Surprisingly, the gene encoding CASPR did not showed any substantial reduction of transcription after rotenone treatment. Of the genes examined, only CAV2 (caveolin 2 gene) displayed a degree of change equivalent to the Contactin 1 and 2 genes. No significant changes were observed for nuclear DNA-encoded complex I subunits, NDUFV1 and NDUFV2, as well as mtDNA-encoded complex I subunit, ND4. OPA1 encodes a protein that plays a crucial role in fusion, fission mechanisms of the mitochondria and its dysfunction has been reported to be associated with diseases of the visual pathway (Bosley et al., 2011; Yu-Wai-Man et al., 2011). OPA1 gene did not seem to be affected by rotenone in the retinal ganglion cells. In order to confirm the genetic data obtained, contents of the proteins in the RGC have been measured. The amounts of contactin and caveolin proteins in the optic nerve were assessed using Western blotting (Fig. 7B) and sections of the retina

were stained with specific antibodies to evaluate the content and location of both proteins (Fig. 7C). It can be seen that rotenone-treated rats exhibited a reduced level of contactin and caveolin both in the optic nerve and RGC layer and that the animals that received Ndi1 displayed a normal level of those proteins.

Discussion

The current work along with our previous finding showed that delivery of complex I inhibitor, rotenone, into the visual pathway of rats gave rise to optic atrophy. We demonstrated that the detrimental effects exerted by rotenone were completely preventable, or can be reversed, by expressing the yeast Ndi1. Similar results of the rotenone administration have been reported using mice (Chadderton et al., 2012). Therefore, under the conditions employed, the action of rotenone is most likely specific to mitochondrial complex I.

One may well expect that the loss of vision was due to RGC death (Saadati et al., 1998; Sadun et al., 2000). In the present study, inhibiting complex I in the visual pathway with rotenone revealed no sign of RGC death and yet visual loss occurred (see also (Marella et al., 2010)). The expression of the Ndi1 protein in the visual pathway was sufficient enough to induce a full recovery of the sight in the rotenone-treated animals, indicating that most of the RGC were still present. In other words, these results suggest that the visual loss caused by complex I inhibition may be ascribed to alteration of the physiology of neurons rather than their death.

One key observation relating to the visual loss was demyelination of the axon of the optic nerve caused by rotenone. Figure 8 illustrates the structure in and around the node of Ranvier and summarizes a possible explanation for the events triggered by complex I inhibition. It is considered that in the central nervous system the Nav channel clusters at nodes of Ranvier are stabilized by two factors: (i) restriction of their lateral mobility by the paranodal junction; (ii) links to the axonal cytoskeleton scaffolds (Susuki and Rasband, 2008). In the optic nerve of rats, rotenone seems to cause disorganization of the node of Ranvier (formation of (CASPR(paranode)-Nav(node))n-CASPR(paranode) repeats). Interestingly the disorganization involved the nodal and paranodal regions but not the juxtaparanode. These morphological changes were well correlated with the visual loss. Question is how structural changes of the nodes of Ranvier lead to a loss of vision. In the paranode, CASPR and contactin are tightly bound to each other to assure anchorage with their myelin counterpart, neurofascin 155 (Zoupi et al., 2011) (Fig. 8, left panel). We demonstrated ROS-dependent disruption of this connection. The disruption might result from oxidative alteration of the protein itself because a tight correlation has been seen between the loss of colocalization and the increase of the oxidative carbonylation of proteins. We also observed lower levels of contactin mRNA and proteins in the RGC of rotenone-treated animals. Given the important role of contactin and CASPR as linkers between the paranodal loop and the axon, it is conceivable that demyelination caused by rotenone seems to act as a causable factor for visual loss.

In addition, the disorganization of the node of Ranvier could result from the perturbation of the paranodal lipid rafts. (Schafer et al., 2004; Ogawa and Rasband, 2009). RT-PCR from laser micro-dissection of the ganglion cell layer and western blot showed a decrease of the caveolin content in the rotenone exposed visual pathway. Caveolins are membranous proteins mainly found in lipid rafts (Fig. 8, left panel). Their principal function is to form special invaginations called caveolae involved in endocytosis and signal transduction (Anderson, 1998; Lajoie and Nabi, 2010). The contactin protein is bound to membranes via a glycosylphosphatidylinositol (GPI)-anchor (Gennarini et al., 1989). GPI-anchored proteins

are associated with glycosphingolipids and cholesterol, principal constituents of lipid rafts. Alteration of the caveolin system can decrease the turnover of GPI-anchored proteins at the plasma membrane and alter the lipid raft integrity (Di Vizio et al., 2008; Pike et al., 2002). Consequently the caveolin proteins could be involved in the overall stability of contactin into the paranodal region. Moreover, it has been shown that the good structure of the paranode depends on the integrity of lipid rafts (Schafer et al., 2004).

We have shown here that impaired complex I in the visual system resulted in loss of the intact structure of the node of Ranvier. The dynamic plasticity of the node of Ranvier is tightly linked to the visual ability of the animals. The relationship between the architecture of the node of Ranvier and the mitochondrial physiology broadens our understanding and may eventually help us develop therapeutic strategies in certain neurodegenerative diseases of the visual pathway.

Conclusions

This study highlights that the visual loss caused by inhibition of mitochondrial complex I is due to an impaired physiology of the retinal ganglion cells. ROS overproduction caused by rotenone induced disorganization of the node of Ranvier and generated demyelination of RGC by disrupting links between myelin and the RGC axon. To repair disorganization of the node of Ranvier seems to be a key factor to rescue the animals from visual loss caused by mitochondrial complex I dysfunction.

Supplementary Material

Refer to Web version on PubMed Central for supplementary material.

Acknowledgments

We thank Dr. Prem Sinha and Motoaki Sato for discussion. This work was supported by U.S. Public Health Service Grants R01EY020796 (to T.Y. and A.M.-Y.).

References

Abramoff MD, Magelhaes PJ, Ram SJ. Image processing with imageJ. Biophotonics International. 2004; 11:36–42.

Anderson RG. The caveolae membrane system. Annu Rev Biochem. 1998; 67:199–225. [PubMed: 9759488]

Bosley TM, Hellani A, Spaeth GL, Myers J, Katz LJ, Moster MR, Milcarek B, Abu-Amero KK. Down-regulation of OPA1 in patients with primary open angle glaucoma. Mol Vis. 2011; 17:1074–1079. [PubMed: 21552501]

Chadderton N, Palfi A, Millington-Ward S, Gobbo O, Overlack N, Carrigan M, O'reilly M, Campbell M, Ehrhardt C, Wolfrum U, Humphries P, Kenna PF, Jane FG. Intravitreal delivery of AAV-NDI1 provides functional benefit in a murine model of Leber hereditary optic neuropathy. Eur J Hum Genet. 2012; 21:68.

Correia SC, Santos RX, Perry G, Zhu X, Moreira PI, Smith MA. Mitochondrial importance in Alzheimer's, Huntington's and Parkinson's diseases. Adv Exp Med Biol. 2012; 724:205–221. [PubMed: 22411245]

Di Vizio D, Adam RM, Kim J, Kim R, Sotgia F, Williams T, Demichelis F, Solomon KR, Loda M, Rubin MA, Lisanti MP, Freeman MR. Caveolin-1 interacts with a lipid raft-associated population of fatty acid synthase. Cell Cycle. 2008; 7:2257–2267. [PubMed: 18635971]

Drose S, Brandt U. Molecular mechanisms of superoxide production by the mitochondrial respiratory chain. Adv Exp Med Biol. 2012; 748:145–169. [PubMed: 22729857]

Filosto M, Tomelleri G, Tonin P, Scarpelli M, Vattemi G, Rizzuto N, Padovani A, Simonati A. Neuropathology of mitochondrial diseases. Biosci Rep. 2007; 27:23–30. [PubMed: 17541738]

Gennarini G, Cibelli G, Rougon G, Mattei MG, Goridis C. The mouse neuronal cell surface protein F3: a phosphatidylinositol-anchored member of the immunoglobulin superfamily related to chicken contactin. J Cell Biol. 1989; 109:775–788. [PubMed: 2474555]

Hildebrand C, Remahl S, Persson H, Bjartmar C. Myelinated nerve fibres in the CNS. Prog Neurobiol. 1993; 40:319–384. [PubMed: 8441812]

Iwata M, Lee Y, Yamashita T, Yagi T, Iwata S, Cameron AD, Maher MJ. Structure of yeast Ndi1 reveals overlapping binding sites for water- and lipid-soluble substrates. Proc Natl Acad Sci U S A. 2012; 109:15247–15252. [PubMed: 22949654]

Joseph AM, Joanisse DR, Baillot RG, Hood DA. Mitochondrial dysregulation in the pathogenesis of diabetes: potential for mitochondrial biogenesis-mediated interventions. Exp Diabetes Res. 2012; 2012:642038. [PubMed: 22203837]

Kazarinova-Noyes K, Shrager P. Molecular constituents of the node of Ranvier. Mol Neurobiol. 2002; 26:167–182. [PubMed: 12428754]

Labasque M, Faivre-Sarrailh C. GPI-anchored proteins at the node of Ranvier. FEBS Lett. 2009; 584:1787–1792. [PubMed: 19703450]

Lajoie P, Nabi IR. Lipid rafts, caveolae, and their endocytosis. Int Rev Cell Mol Biol. 2010; 282:135–163. [PubMed: 20630468]

London E, Brown DA. Insolubility of lipids in triton X-100: physical origin and relationship to sphingolipid/cholesterol membrane domains (rafts). Biochim Biophys Acta. 2000; 1508:182–195. [PubMed: 11090825]

Manders EMM, Verbeek FJ, Aten JA. Measurement of co-localization of objects in dual-colour images. J Microscopy. 2013; 169:375–382.

Marella M, Seo BB, Matsuno-Yagi A, Yagi T. Mechanism of cell death caused by complex I defects in a rat dopaminergic cell line. J Biol Chem. 2007; 282:24146–24156. [PubMed: 17581813]

Marella M, Seo BB, Nakamaru-Ogiso E, Greenamyre JT, Matsuno-Yagi A, Yagi T. Protection by the *NDI1* Gene against Neurodegeneration in a Rotenone Rat Model of Parkinson's Disease. PLoS ONE. 2008; 3:e1433. [PubMed: 18197244]

Marella M, Seo BB, Thomas BB, Matsuno-Yagi A, Yagi T. Successful amelioration of mitochondrial optic neuropathy using the yeast *NDI1* gene in a rat animal model. PLoS ONE. 2010; 5:e11472. [PubMed: 20628600]

Murphy MP. How mitochondria produce reactive oxygen species. Biochem J. 2009; 417:1–13. [PubMed: 19061483]

Nunnari J, Suomalainen A. Mitochondria: in sickness and in health. Cell. 2012; 148:1145–1159. [PubMed: 22424226]

Ogawa Y, Rasband MN. Proteomic analysis of optic nerve lipid rafts reveals new paranodal proteins. J Neurosci Res. 2009; 87:3502–3510. [PubMed: 19156860]

Pike LJ, Han X, Chung KN, Gross RW. Lipid rafts are enriched in arachidonic acid and plasmenylethanolamine and their composition is independent of caveolin-1 expression: a quantitative electrospray ionization/mass spectrometric analysis. Biochemistry. 2002; 41:2075–2088. [PubMed: 11827555]

Saadati HG, Hsu HY, Heller KB, Sadun AA. A histopathologic and morphometric differentiation of nerves in optic nerve hypoplasia and Leber hereditary optic neuropathy. Arch Ophthalmol. 1998; 116:911–916. [PubMed: 9682705]

Sadun AA, Win PH, Ross-Cisneros FN, Walker SO, Carelli V. Leber's hereditary optic neuropathy differentially affects smaller axons in the optic nerve. Trans Am Ophthalmol Soc. 2000; 98:223–232. [PubMed: 11190025]

Salzer JL. Polarized domains of myelinated axons. Neuron. 2003; 40:297–318. [PubMed: 14556710]

Schafer DP, Bansal R, Hedstrom KL, Pfeiffer SE, Rasband MN. Does paranode formation and maintenance require partitioning of neurofascin 155 into lipid rafts? J Neurosci. 2004; 24:3176–3185. [PubMed: 15056697]

Schapira AH. Human complex I defects in neurodegenerative diseases. Biochim Biophys Acta. 1998; 1364:261–270. [PubMed: 9593927]

Schroeder RJ, Ahmed SN, Zhu Y, London E, Brown DA. Cholesterol and sphingolipid enhance the Triton X-100 insolubility of glycosylphosphatidylinositol-anchored proteins by promoting the

formation of detergent-insoluble ordered membrane domains. J Biol Chem. 1998; 273:1150–1157. [PubMed: 9422781]

Seo BB, Marella M, Yagi T, Matsuno-Yagi A. The single subunit NADH dehydrogenase reduces generation of reactive oxygen species from complex I. FEBS Lett. 2006a; 580:6105–6108. [PubMed: 17055488]

Seo BB, Nakamaru-Ogiso E, Flotte TR, Matsuno-Yagi A, Yagi T. *In vivo* complementation of complex I by the yeast Ndi1 enzyme: possible application for treatment of Parkinson disease. J Biol Chem. 2006b; 281:14250–14255. [PubMed: 16543240]

Sherer TB, Richardson JR, Testa CM, Seo BB, Panov AV, Yagi T, Matsuno-Yagi A, Miller GW, Greenamyre JT. Mechanism of toxicity of pesticides acting at complex I: relevance to environmental etiologies of Parkinson's disease. J Neurochem. 2007; 100:1469–1479. [PubMed: 17241123]

Smith RA, Hartley RC, Cocheme HM, Murphy MP. Mitochondrial pharmacology. Trends Pharmacol Sci. 2012; 33:341–352. [PubMed: 22521106]

Sproule DM, Kaufmann P. Mitochondrial encephalopathy, lactic acidosis, and strokelike episodes: basic concepts, clinical phenotype, and therapeutic management of MELAS syndrome. Ann N Y Acad Sci. 2008; 1142:133–158. [PubMed: 18990125]

Stefanatos R, Sanz A. Mitochondrial complex I: A central regulator of the aging process. Cell Cycle. 2011; 10:1528–1532. [PubMed: 21471732]

Susuki K, Rasband MN. Molecular mechanisms of node of Ranvier formation. Curr Opin Cell Biol. 2008; 20:616–623. [PubMed: 18929652]

Yu-Wai-Man P, Bailie M, Atawan A, Chinnery PF, Griffiths PG. Pattern of retinal ganglion cell loss in dominant optic atrophy due to OPA1 mutations. Eye (Lond). 2011; 25:596–602. [PubMed: 21378995]

Zhang X, Jones D, Gonzalez-Lima F. Mouse model of optic neuropathy caused by mitochondrial complex I dysfunction. Neurosci Lett. 2002; 326:97–100. [PubMed: 12057837]

Zoupi L, Savvaki M, Karagogeos D. Axons and myelinating glia: An intimate contact. IUBMB Life. 2011; 63:730–735. [PubMed: 21793162]

Abbreviations

complex I	mitochondrial proton-translocating NADH-quinone oxidoreductase
Ndi1	internal rotenone-insensitive NADH-quinone oxidoreductase of *Saccharomyces cerevisiae* mitochondria
RGC	retinal ganglion cell
SC	superior colliculus
VC	visual cortex
AAV2-NDI1	adeno-associated virus carrying the *NDI1* gene
mtDNA	mitochondrial DNA
8-oxo-dG	7,8-dihydro-8-oxo-deoxyguanine
ROS	reactive oxygen species

Highlights

- Complex I inhibition of the visual pathway leads to nodal disorganization.
- The anchorage proteins of the nods were impacted.
- Disorganization of the nodal structure was tightly linked to visual impairment.
- The present study may lead to therapeutic interventions for optic neuropathy.

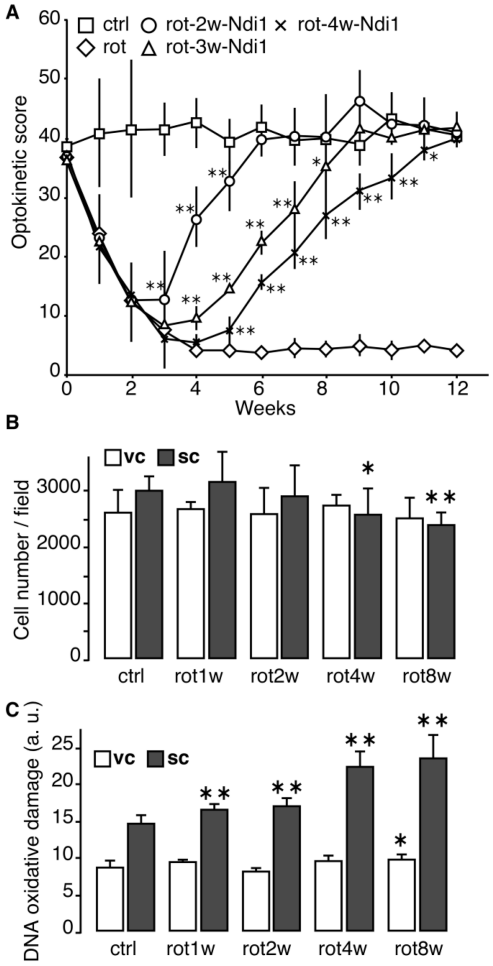

Fig. 1. Optokinetic score of rats and evaluation of the neuronal population in the VC

A, The vision of rats was assessed once every week for 12 weeks. The animals performed the optokinetic test for 2 minutes and the time of head tracking was recorded. When specified the rats received an AAV2-NDI1 injection at the same stereotaxic coordinates as those for the rotenone microspheres at least 2 days before being tested again. Square = control; diamond = rotenone; circle = AAV2-NDI1 after 2 weeks of rotenone exposure; triangle = AAV2-NDI1 after 3 weeks of rotenone exposure; cross = AAV2-NDI1 after 4 weeks of rotenone exposure. B, Sagittal sections of rat brains were stained with the antibody against neuron specific protein, NeuN. Positive cells in the SC and the VC were counted and the results were compiled into histograms. C, Sagittal sections of rat brains were stained with the 8-oxo-dG antibody. The relative intensities of the staining were compiled into histograms. The cell count and fluorescence evaluation were performed on 3 different animals per group. 4 brain sections separated by at least 150μm were used per animal. * $p \leq 0.05$; ** $p \leq 0.01$ (one way ANOVA).

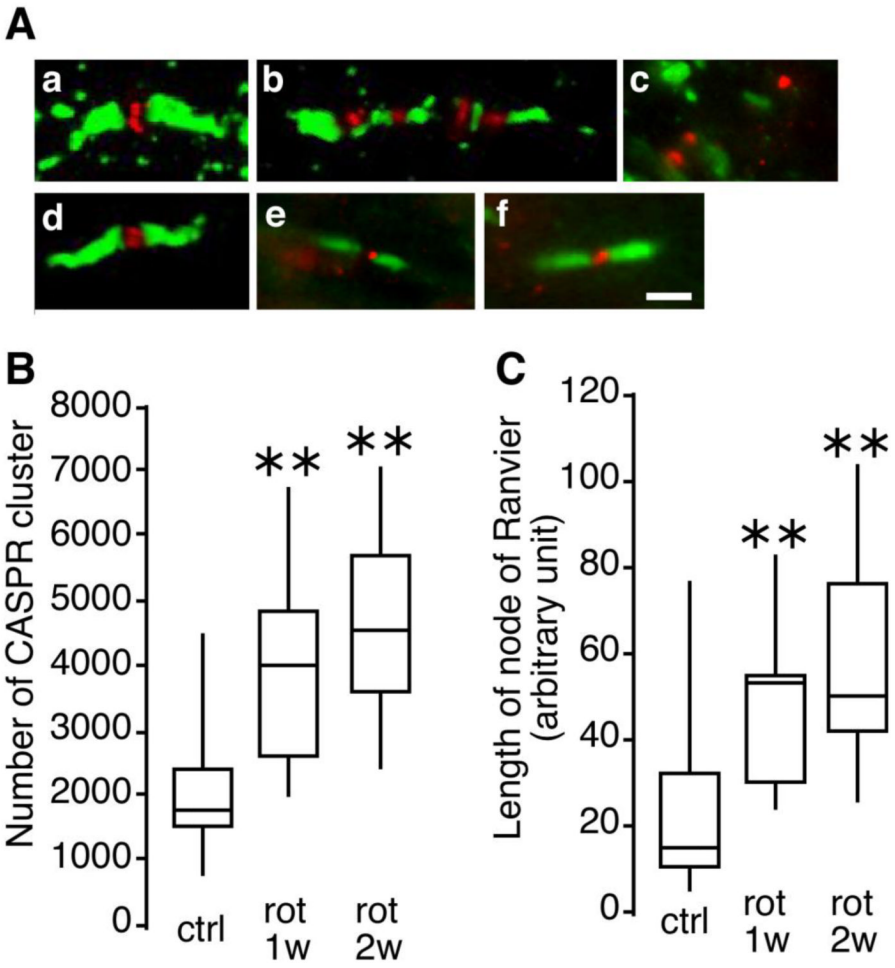

Fig. 2. Shape of the node of Ranvier and characterization of CASPR clusters in the rat optic nerve

Thin sections (5μm) of rat optic nerves were stained with antibodies against CASPR (green) and sodium channels (NaV1.6, red) to reveal nodes of Ranvier. A, representative images of the node of Ranvier observed by three dimensional confocal microscopy. a, a typical image of the normal node of Ranvier (observed in control animals). b, an elongated node of Ranvier (observed at 2 weeks after rotenone injection). c, a totally disorganized node of Ranvier (observed at 12 weeks after rotenone injection). d, e, and f, representative patterns of the node of Ranvier from animals that received AAV2-NDI1, respectively, 2 week, 3 weeks, and 4 weeks after rotenone injection. Scale bar = 2 μm. B, the number of CASPR clusters counted in optic nerve sections and compiled in a box plot. C, the length of the node of Ranvier evaluated and compiled in a box plot. For B and C the evaluation was performed on 3 different animals per group. 32 sections of the left and right optic nerves were used per animal ** $p<0.01$ (one way ANOVA).

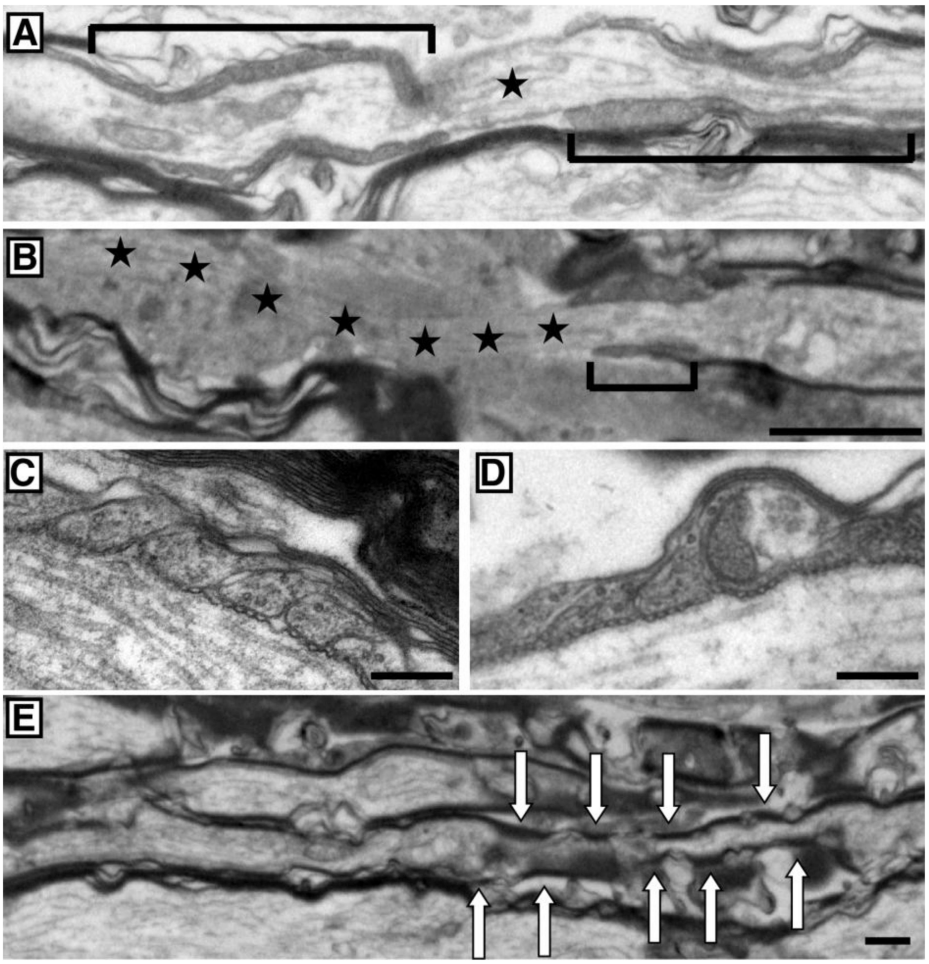

Fig. 3. Ultra structure of the node of Ranvier

Representative images of sagittal sections of the rat optic nerve observed under electron microscope are displayed. A and B, the nodal region from a control group (A) and a group treated with rotenone for 4 weeks (B). The brackets denote the paranodal region surrounding the node of Ranvier. The stars mark the node of Ranvier (uncovered portion of the axon). In the rotenone-treated group, a smaller paranode region indicating a thinner myelin is seen and a mirrored paranode section was not observed resulting in a large region of uncovered axon (stars). C and D, the paranodal ending loops of the myelin sheath from a control group (C) and a group treated with rotenone for 4 weeks (D). E, the nodal region from a group treated with rotenone for 4 weeks illustrating discontinued myelination of an axon (highlighted by arrows). Scale bar = 1μm for A, B and E and 250nm for C and D.

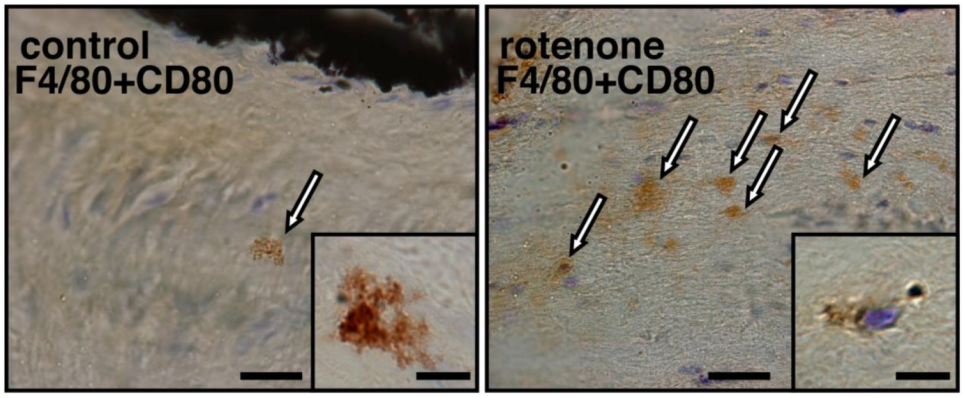

Fig. 4. Microglial invasion of the optic nerve in rotenone-treated rats

Optic nerve samples were collected after 4 weeks of rotenone exposure. Longitudinal sections were stained with antibodies against F4/80 and CD80 and representative images are displayed. Activated microglial cells (amoeboid shape, marked by arrows) were abundant in the rotenone-treated animals. Scale bar = 30 μm. Inserts: images of microglia at a higher magnification. In the control sample, most microglia appeared highly ramified. In the optic nerve of the rotenone-treated animals, the microglial cells lost their numerous cytoplasmic expansions. Scale bar = 7 μm.

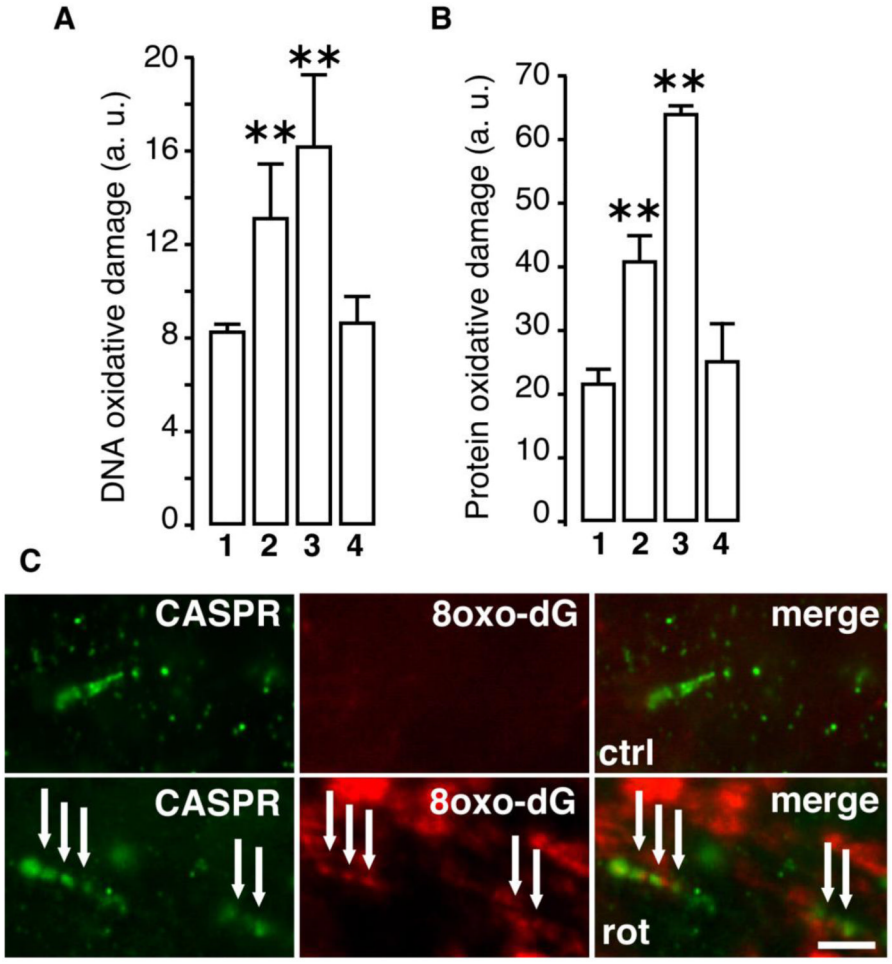

Fig. 5. Oxidative damage of the optic nerve

Sagittal sections of the optic nerve were stained with antibody against 8-oxo-dG (A) and 2,4 DNP (B) to assess the oxidation of DNA and proteins, respectively (representative images provided in Supplementary Fig. 6). The extent of oxidative damage was compiled into histograms by measuring the staining intensity using ImageJ software (Abramoff et al., 2004). 1, control animals. 2, rotenone two weeks. 3, rotenone three weeks. 4, injection of AAV2-NDI1 after four weeks of rotenone exposure. The oxidative damage in 4, was evaluated after four weeks of Ndi1 expression. C shows high magnification pictures of the optic nerve from a control group (upper panel) and a group treated with rotenone for two weeks (lower panel). The oxidation of DNA was shown with 8-oxo-dG staining (red). The paranode section of the node of Ranvier was revealed by anti-CASPR antibody (green). Scale bar=5μm. For A and B, fluorescence evaluation were performed on 3 different animals per group. 8 optic nerve section separated by at least 48 μm were used per animal. * $p \leq 0.05$; ** $p \leq 0.01$ (one way ANOVA).

A

Conditions	Mander's coeficient
Control	0.965±0.026
Rotenone 2 weeks	0.873±0.038**
Rotenone 4 weeks	0.765±0.010**
Rotenone 12 weeks	0.717±0.042**
Rotenone 2 weeks + Ndi1	0.937±0.046
Rotenone 3 weeks + Ndi1	0.980±0.005
Rotenone 4 weeks + Ndi1	0.960±0.027

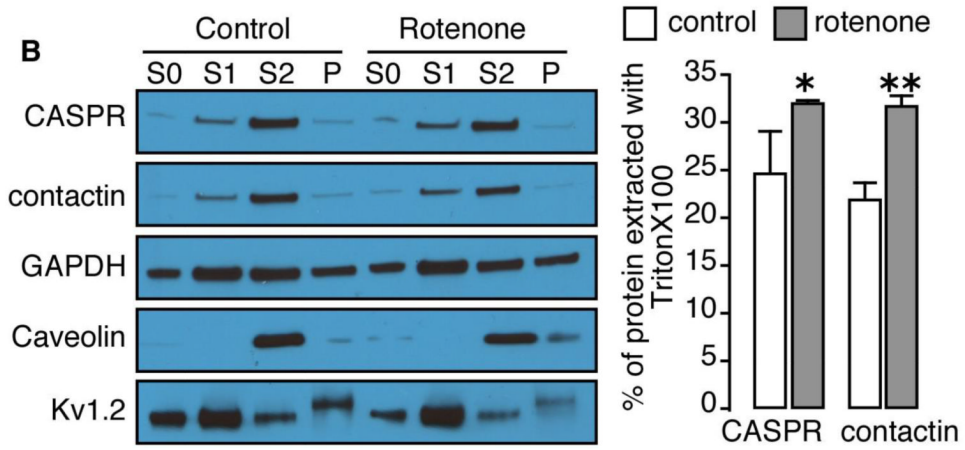

Fig. 6. Evaluation of colocalization of CASPR and contactin in the optic nerve of rotenone-treated rats

A, immunofluorescence staining for CASPR and contactin was carried out on thin sections of the rat optic nerves as illustrated in Supplementary Fig. 7. Mander's coefficients of colocalization of the red color (contactin) and the green color (CASPR) were then calculated and summarized in a table. The Mander's coefficient is an index for overlapping pixels between two colors with 1.0 being a perfect colocalization. The samples were collected after 2, 4, and 12 weeks of rotenone exposure. When Ndi1 was expressed, the samples were processed at week 12 of the experiment. Evaluation was performed on 3 different animals per group. 32 sections of the left and the right optic nerves were used per animal. * $p \leq 0.05$; ** $p \leq 0.01$ (one way ANOVA). B, TritonX-100-dependent extraction of CASPR and contactin from the optic nerve followed by a series of fractionation was carried out on the animals treated with rotenone for 4 weeks (see Materials and Methods for details). The amounts of CASPR and contactin in the pellet and supernatant fractions were evaluated by Western blot analysis using the antibodies indicated. S0 represents the initial material of mashed optic nerves before the fractionation, S1 represents the supernatant fraction after extraction with TritonX-100 at 4°C for 30 min, S2 represents the pellet fraction from the Triton X-100 extraction that was dissolved in SDS, and P represents the fraction of insoluble proteins after the SDS treatment. C, percentage of protein extracted with Triton X-100 was assessed and compiled in histograms by using the equation: % of protein extracted with TritonX-100 = (S1 density/(S1 density + S2 density)) × 100. The data were from analysis of 3 runs of Western Blots derived from the optic nerves from 3 different rats.

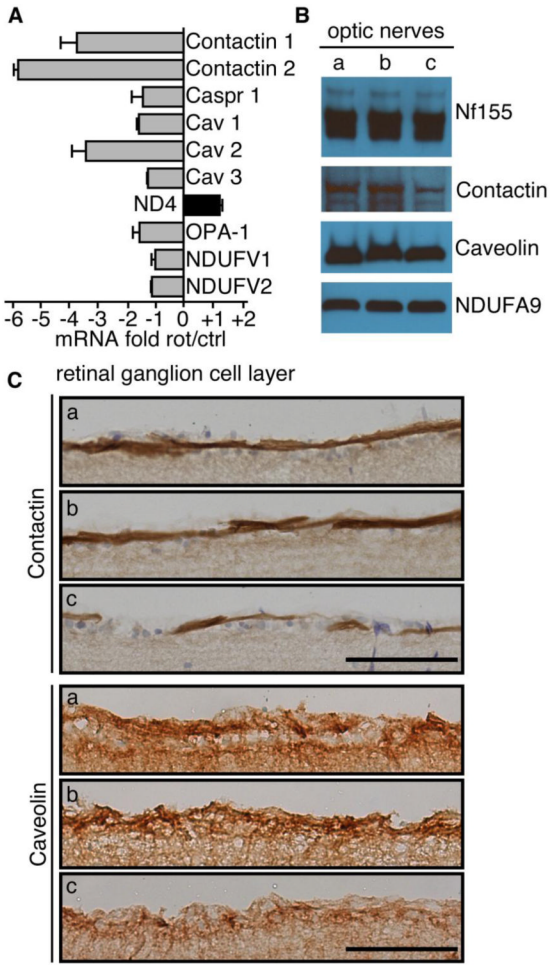

Fig. 7. Evaluation of contents of specific mRNA and proteins in the visual pathway of rats

A, the mRNA contents in the ganglion cell layer after laser-capture-microdissection: RT-PCR was performed after microdissection of the ganglion cell layer 2 weeks after rotenone administration. The mRNA content of the gene was determined from 3 animals and 12 retina sections per animal. The values represent average ratios between the rotenone-treated and the control animals (negative values mean a decrease of mRNA in the rotenone group). B, representative Western-Blot of neurofascin 155 (Nf155), contactin, and caveolin proteins in the whole optic nerve preparation. Complex I subunit Ndufa9 was used as control. C, Rat retinas were stained to evaluate the content of contactin and caveolin in the ganglion cell layer. Scale bar = 50 μm. In B and C the following groups were examined. a, control rats; b, rats treated with rotenone for 2 weeks followed by an AAV2-NDI1 injection; c, rats treated with rotenone for 2 weeks.

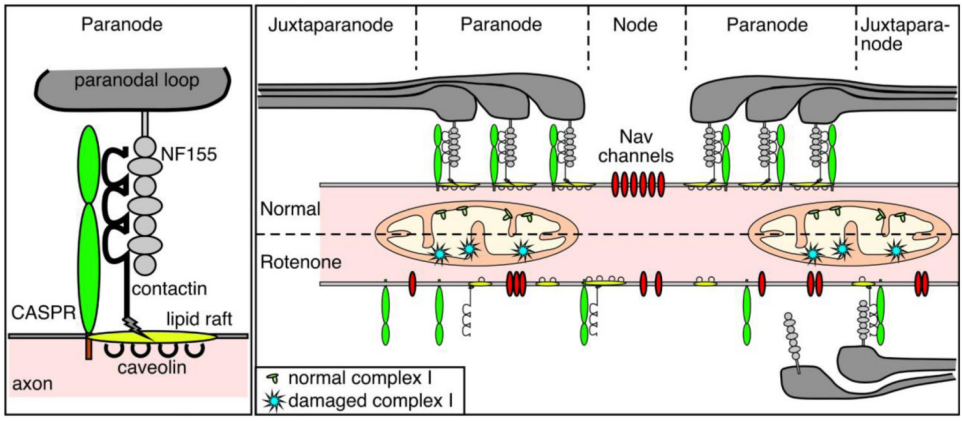

Fig. 8. Disorganization of the node of Ranvier after complex I inhibition

The cartoon represents the organization of the main anchorage protein system at the node of Ranvier location. In a normal situation the myelin ending loops (paranodal loop) are attached via the binding of CASPR, contactin on the axon and NF155 on the myelin sheath. All the nodal components are therefore well segregated. When mitochondrial complex I is affected, the anchorage proteins cannot maintain their function and the binding between myelin and the axon is lost. The node of Ranvier becomes disorganized. The sodium channels invade the paranodal region. The saltatory conduction can no longer be ensured, which results in a decrease of the visual capacity.